Contemporary Mathematics
https://ojs.wiserpub.com/index.php/CM/

Research Article

Local Wavelet Transform on a Helix Space Curve Based on Frenet Frame

Xiaohui Zhou[1*], Jian Zhu[2]

[1]Department of Finance and AI Research Center, Shanghai University of Finance and Economics-Zhejiang College, Jinhua Zhejiang, 321000, China
[2]Department of Mathematics and Physics, Xinjiang Institute of Engineering, Urumqi, 830023, China
E-mail: zhou001900@163.com

Received: 26 May 2025; **Revised:** 1 September 2025; **Accepted:** 10 September 2025

Abstract: Based on the Frenet frame, the approximate Local Wavelet Transform (LWT) is investigated on a class of generalized helix curves by their tangent projections at specific points. Initially, parametric equations are formulated for various types of helix curves, including circular helices and generalized helices. A particular helix curve on a unit sphere is selected as a representative instance of a generalized helix, and its tangent projection at a designated point is computed. Subsequently, the dilation and translation operators for a wavelet function are rigorously defined to facilitate the study of the LWT on this curve. A corresponding reconstruction formula is also derived. The Morlet wavelet is projected onto the space curve at the specified point $t = 0$ by the tangent projection method. To validate the proposed approach, three numerical examples are presented, demonstrating the application of the LWT and its inverse LWT (reconstruction formula) to analyze localized signals. The simulation results are illustrated through graphical representations.

***Keywords*:** Local Wavelet Transform (LWT), circular helix curve, tangent projection

MSC: 42C40, 65T60, 53A04

1. Introduction

Wavelet method has undergone rapid and significant advancements. It excels in processing non-stationary data, providing temporal localization, and conducting multi-scale signal analysis. The application of wavelet analysis spans diverse fields, encompassing signal analysis, image processing, object and facial recognition [1, 2], financial analysis [3, 4], and more. Real-world data often resides on specific smooth manifolds, such as hyperboloids, paraboloids, and various other two-dimensional smooth manifolds [5, 6], as well as abstract manifolds. One promising approach to studying wavelets on manifolds leverages Lie groups theory and corresponding representation. For instance, many scholars such as Singh and Bhate, Leduc, Kikuchi and Wang, explored Continuous Spatiotemporal Wavelet Transform (CSWT) through unitary representations of kinematic groups [7–9]. The CSWT are prevalent in detecting the missile warhead [8] and tracking, as well as in analyzing multi-scale geophysical phenomena [9, 10] and a specific type of stochastic wavelet [7].

An alternative method to discuss wavelets and their applications on manifolds [4–6] involves some special bijective projections, such as vertical projection, stereographic projection, and length-preserving projection. Building on wavelet

DOI: https://doi.org/10.37256/cm.6620257299

methods tailored to specific curves, novel interpretations emerge in handling financial data (e.g., Bitcoin transactions, financial institution deposit balances), including concepts like 'volatility relative to regression growth trends', 'errors in regression growth trends', and 'wavelet approximations along regression trend lines' [4]. These financial data manipulations primarily focus on planar curves, like linear regression curves [4] and logarithmic curves. Additionally, numerous real-world datasets inhabit space curves, such as flight trajectories and satellite orbits, primarily residing on spherical space curves, other helix and so on. Helix is ubiquitous in nature and daily life, showcasing remarkable adaptability and aesthetic value. In biological systems, Deoxyribonucleic Acid (DNA)'s double helix stores genetic information, protein α helix provide structural functions, while vines utilize spiral growth to optimize spatial utilization. In human applications, helix staircases maximize space efficiency, screw threads ensure secure fastening, and springs harness elastic energy storage. Celestial phenomena such as galactic helix and tornadoes, along with helix motifs in artistic sculptures, all exemplify the dynamic equilibrium and visual harmony inherent in a helix. When analyzing and processing the information and data on these helix, wavelet methods must be adapted to these helix curves. This paper delves into local wavelet transforms for dealing with local signal on a specific helix curve.

The structure of this paper is as follows: Section 2 introduces preliminaries, including definitions of helix curves and local bijective projections on generalized helices. Section 3 discusses local continuous wavelet transforms on generalized helices using local bijective projections and local dilations, deriving a reconstruction formula. Finally, we present two illustrative examples and figures to explore wavelets on space curves and their applications.

2. Preliminary

Firstly, some helix curves are introduced, some local tangent projection are also computed in the section.

2.1 *Parametric equation of generalized helix curves*

The mathematical description of a cylindrical helix arises from the superposition of two orthogonal kinematic components: a uniform rotational motion about a fixed axis and a uniform translational displacement along the same axis. This helical trajectory, characterized by cylindrical symmetry, is fundamental in mechanical engineering and dynamical systems analysis. The parametric equations governing this motion can be expressed in Cartesian coordinates as:

$$\vec{\rho} = \left\{ r\cos(\theta),\ r\sin(\theta),\ \frac{p}{2\pi}\theta \right\},$$

where r denotes the constant radius of the circular motion, θ represents the angular displacement parameter, p corresponds to the helical pitch-the axial distance between consecutive turns. The temporal parameter t relates to the angular coordinate through $\theta = \omega t$, with ω being the constant angular velocity. The proposed kinematic system constitutes a non-holonomic superposition of two orthogonal rotational motions, generating a compound helical trajectory with dual periodicity. This configuration, analogous to hierarchical orbital systems in astrophysics (e.g., Earth-Moon-Sun dynamics). Similar to the equation of a circular helix, the parametric formulation in a space vector is introduced and defined as follows.

Definition 1 [11, 12] Assume that the kinematic trajectory of a space particle satisfies the following parametric formulation:

$$\vec{\rho} = \{(r + \upsilon_0\cos(\omega t))\cos(t),\ (r + \upsilon_0\cos(\omega t))\sin(t),\ \upsilon_0\sin(\omega t)\} \tag{1}$$

where $|\upsilon_0| < r$, r represents the radius of the first rotational motion parallel to the XOY plane, υ_0 denotes the radius of the second rotational motion orthogonal to the first one, ω is an angular parameter, then this kinematic trajectory is a circular helix.

If the first rotational motion becomes an elliptic in Eq. (1), an elliptic helix is introduced in the following Definition 2.

Definition 2 [11, 12] Assume that thekinematic trajectory of a space particle satisfies the following parametric formulation:

$$\vec{\rho} = \{(r_1 + \upsilon_0 \cos(\omega t))\sec(t),\ (r_2 + \upsilon_0 \cos(\omega t))\tan(t),\ \upsilon_0 \sin(\omega t)\} \tag{2}$$

where $|\upsilon_0| < r_1$, r_1, r_2 are the long half axis and the short half axis of an ellipse and υ_0 denotes the radius of the circle, ω is the angular speed, then the trajectory is a elliptic helix.

Generalizing the Definition 1 and 2, we have

Definition 3 [11, 12] Consider a plane continuous curve, and its parametric formulation is

$$\begin{cases} f = x(t) \\ g = y(t) \end{cases}, \ t \text{ is a parameter.}$$

If a kinematic trajectory of a space particle satisfies the parametric formulation:

$$\vec{\rho} = \{(r + v_0 \cos(\omega t))x(t),\ (r + v_0 \cos(\omega t))y(t),\ v_0 \sin(\omega t)\} \tag{3}$$

where r, v_0, ω are constants satisfying some conditions, it is called a class of generalized helix.

According to these parametric formulation, the adjacent structure of a generalized helix curve at one point can be established based on its Frenet frame, which can be computed by frame's vectors:

$$\vec{\alpha} = \frac{\vec{\rho}'}{|\vec{\rho}'|},\ \vec{\gamma} = \frac{\vec{\rho}' \times \vec{\rho}''}{|\vec{\rho}' \times \vec{\rho}''|},\ \beta = \vec{\gamma} \times \vec{\alpha}. \tag{4}$$

Example 1 Consider the parameters $r = 0$, $\upsilon_0 = 1$, $\omega = 1$ and $x(t) = \cos 2t$, $y(t) = \sin 2t$ in the formula (3). So the parametric formulation of this special helix curve is shown as the following equation:

$$\vec{\rho} = \{\cos t \cos 2t,\ \cos t \sin 2t,\ \sin t\}$$

From the parametric equation, this special helix is a curve in a unit sphere. Figure 1 shows its figure as the blue curve. The tangent vector of $\vec{\rho}$ is

$$\vec{\rho}' = \{-\sin t \cdot \cos(2t) - 2\cos t \cdot \sin 2t,\ 2\cos t \cdot \cos(2t) - \sin t \cdot \sin 2t,\ \cos t\} \tag{5}$$

For an arbitrary given point t_0, $\vec{\rho}(t_0) \cdot \vec{\rho}'(t_0) = 0$, the tangent vector $\vec{\rho}'(t_0)$ is vertical to $\vec{\rho}(t_0)$. Choose $t_0 = \dfrac{\pi}{5}$ and the tangent line's figure at the point $t_0 = \dfrac{\pi}{5}$ is computed from Eq. (5) and shown in the Figure 1. Its Frenet frame of this

helix curve at point $t_0 = \frac{\pi}{5}$ can be generated by computing Eq. (4). However, based on curvature κ_0 and scratch rate τ_0 at $t_0 = \frac{\pi}{5}$, the adjacent points' coordinate (x^*, y^*, z^*) can be represented by

$$x^* = \ell,\ y^* = \frac{1}{2}\kappa_0\ell^2,\ z^* = \frac{1}{2}\kappa_0\tau_0\ell^2,$$

where ℓ denotes the length parameter (seen in Ref. [13, 14]).

Combined the adjacent points' coordinate (x^*, y^*, z^*) and Frenet frame at point $t_0 = \frac{\pi}{5}$, the helix curve's adjacent structure at point $t_0 = \frac{\pi}{5}$ is shown in Figure 2a. Vector $\vec{\alpha}, \vec{\gamma}, \vec{\beta}$ can be seen as vector Alpha, vector Gamma and vector Beta in Figure 2b (Local enlarged adjacent structure of Figure 2a) respectively. A green pecked line implies an approximation of this helix at $t_0 = \frac{\pi}{5}$.

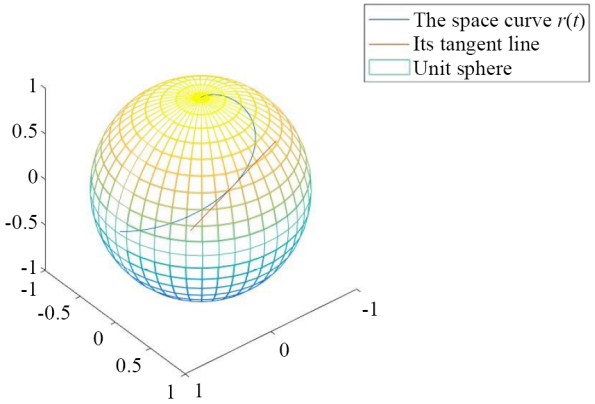

Figure 1. A helix curve and its tangent line at $t_0 = \frac{\pi}{5}$

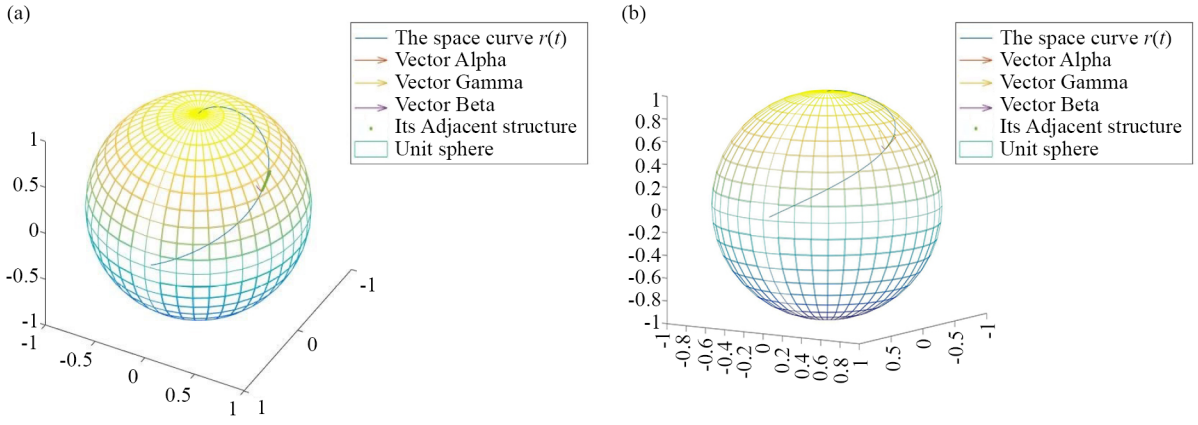

Figure 2. (a) The adjacent structure of the helix curve at point; (b) Local enlarged adjacent structure of Figure 2a

2.2 *Local tangent projection of a helix*

A local orthogonal projection of a vector onto a specified subspace is formally characterized through the inner product operation in Hilbert space theory, as demonstrated by the Riesz representation theorem. Regarding the parametric curve described in Example 1, which exists within the geometric constraints of a unit sphere, the tangent vector at any differentiable point t_0 on this manifold can be systematically derived using the following equation:

$$\vec{\rho}'(t_0) = \{-\sin t_0 \cdot \cos(2t_0) - 2\cos t_0 \cdot \sin 2t_0, 2\cos t_0 \cdot \cos(2t_0) - \sin t_0 \cdot \sin 2t_0, \cos t_0\}$$

So calculate the norm of a vector $|\vec{\rho}'(t_0)| = \sqrt{4\cos^2 t_0 + 1}$. And tangent vector $\vec{\alpha}(t_0)$ at t_0 can be obtained that

$$\vec{\alpha}(t_0) = \frac{\vec{\rho}'(t_0)}{|\vec{\rho}'(t_0)|}$$

The tangent projection from a helix curve onto its tangent line can be generated by the following equation:

$$P : \vec{\rho}(t) \to \vec{\rho}(t_0) + \left\langle \vec{\rho}(t),\ \vec{\alpha}(t_0) \right\rangle \vec{\alpha}(t_0). \tag{6}$$

Based on this tangent projection, the distance between the projection point $\vec{\rho}(t_0) + \langle \vec{\rho}(t),\ \vec{\alpha}(t_0)\rangle \vec{\alpha}(t_0)$ to initial point $\vec{\rho}(t_0)$ is the absolute value of inner product $|\langle \vec{\rho}(t),\ \vec{\alpha}(t_0)\rangle|$. A real axis at the point $\vec{\rho}(t_0)$ as an origin point is generated by this tangent line on the helix curve $\vec{\rho}(t)$. So the tangent projection P is equivalent to the following local projection p:

$$p : t \to T = \left\langle \vec{\rho}(t),\ \vec{\alpha}(t_0) \right\rangle \tag{7}$$

Choose a neighborhood $\left(0,\ \frac{2\pi}{5}\right)$ at point $t_0 = \frac{\pi}{5}$, the corresponding local helix curve is given in the Figure 3. The projected line on this neighborhood is also shown in the Figure 3. Based on this projection p defined as in formula (6), this local helix is mapped to its tangent line at point $t_0 = \frac{\pi}{5}$.

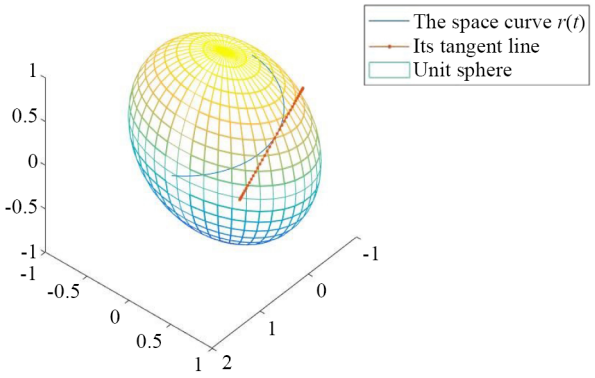

Figure 3. The local helix curve at point $t_0 = \frac{\pi}{5}$ and its projection

3. LWT on a generalized helix

Consider a helix curve C and $\Im = L^2(C,\, d\mu)$ is a Hilbert space on this curve C, with a scaling product $< \cdot,\, \cdot >_{\Im}$ and a measure $d\mu$. The notation $T_\tau(C)$ represents a tangent space at the point $\tau \in C$. For the sake of discussing LWT on a helix curve C, a square integrable function $\psi^{(\tau)} \in \Im$, which is compactly supported, should be given as the mother wavelet basis in a neighborhood $B_{(\tau)},\ \tau \in C$. Moreover, an appropriate local dilation operator should be considered on a helix curve C. In the interest of establishing wavelet basis on a helix curve C through translating and dilating a mother wavelet, an effective approach is to project points in neighborhood $B_{(\tau)},\ \tau \in C$, onto its tangent line. Then the translated and dilated point should be hauled back onto this helix.

Consider a helix C which is satisfied the following parameter formula

$$\tau = \vec{\rho}(t) = (\rho_1(t),\ \rho_2(t),\ \rho_3(t)),\ t \in I \subset R,$$

where $\rho_1(t),\ \rho_2(t),\ \rho_3(t)$ can be obtained in Definition 1-3. For a given point t_0, there is a neighbourhood $\Lambda(t_0)$ such that the local projection p defined in formula (7) is bijective, that is,

$$p_{t_0} : t \mapsto T = \left\langle \vec{\rho}\,(t),\ \vec{\alpha}\,(t_0) \right\rangle \in \Lambda(t_0) \subset R \tag{8}$$

where $\tau_0 = \vec{\rho}\,(t_0)$. So $p_{t_0}(t_0) = T_0 = 0$. Moreover, the components $p_1(t),\ p_2(t),\ p_3(t)$ of the projection vector P can be computed by $\vec{\rho}\,(t_0) + \langle \vec{\rho}(t),\ \vec{\alpha}\,(t_0) \rangle\, \vec{\alpha}\,(t_0)$ in Eq. (6).

Consider the Example 1, since $\langle \vec{\rho}(t),\ \vec{\alpha}\,(t_0) \rangle = \dfrac{1}{\sqrt{4\cos^2 t_0 + 1}} (\cos t \sin(2t - 3t_0) + \cos t \cos t_0 \sin(2t - 2t_0) + \sin t \cos t_0)$ the local coordinates of local projection can be denoted by

$$p_{t_0} : t \mapsto \frac{1}{\sqrt{4\cos^2 t_0 + 1}} (\cos t \sin(2t - 3t_0) + \cos t \cos t_0 \sin(2t - 2t_0) + \sin t \cos t_0)$$

Obviously, p_{t_0} is continuous and there is an interval of point t_0 so that the projection p_{t_0} is a diffeomorphism. At some special points $t_0 = \dfrac{\pi}{2} + k\pi,\ k \in Z$, the above mapping can be rewritten as

$$p_{t_0} : t \mapsto \cos t \sin\left(2t - \frac{3\pi}{2} - 3k\pi\right) = \begin{cases} 2\cos^3 t - 1 & k = 2n \\ 1 - 2\cos^3 t & k = 2n+1 \end{cases}$$

where n is an integer.

Similar to the Refs. [3, 13], a suitable local dilation of local point at t_0 can be defined as

$$d_\alpha : t \mapsto t_\alpha = p_{t_0}^{-1} \cdot \alpha \cdot p_{t_0}, \qquad \alpha > 0$$

Then maximum value of local dilation at t_0 is $\alpha_{\max} = \sup_{t \in \Lambda(t_0)} p_{t_0}$. Thus, $p_{t_0}(t_\alpha) = \alpha \cdot p_{t_0}(t)$

Similar to the Refs. [3, 12], the dilation operator of functions with a compactly support in $B_{(\tau_0)}$ is given to act on a function.

Definition 4 Assume that a subspace of $\mathfrak{I}$ is written as $\mathfrak{I}(B_{(\tau_0)})$. For a given local wavelet function $\psi^{(\tau_0)} \in \mathfrak{I}(B_{(\tau_0)})$, a dilation operator with factor α of $\psi^{(\tau_0)}$ is denoted as the following equation:

$$D_{\tau_0}(\alpha) : \psi^{(\tau_0)}(t) \mapsto \lambda^{\frac{1}{2}}(\alpha,\, t)\psi^{(\tau_0)}(t_{\alpha^{-1}}) \tag{9}$$

where $\tau_0 = \vec{\rho}\,(t_0)$ and $\lambda(\alpha,\, t)$ is the Radon-Nikodym derivative which is defined as

$$\lambda(\alpha,\, t) = \frac{d\mu\,(t_{\alpha^{-1}})}{d\mu(t)} \tag{10}$$

which implicates the variety of the measure μ based on a dilation factor α.

By using the implicit function differential approach, the $\lambda(\alpha,\, t)$ can also be computed by the following equation

$$p_{t_0}(t_\alpha) = \alpha \cdot p_{t_0}(t),$$

then,

$$p'_{t_0}(t_\alpha)\, d\mu\,(t_\alpha) = \alpha \cdot p'_{t_0}(t) d\mu(t).$$

So

$$\lambda(\alpha,\, t) = \frac{d\mu\,(t_{\alpha^{-1}})}{d\mu(t)} = \frac{\alpha^{-1} p'_{t_0}(t)}{p'_{t_0}(t_{\alpha^{-1}})}. \tag{11}$$

Assume that there is a $t^{\#}_{\alpha^{-1}}$ so that $p_{t_0}\left(t^{\#}_{\alpha^{-1}}\right) = \alpha^{-1} \cdot p_{t_0}(t) - p(t)$, where $\vec{\rho}(t) \in C$,

$$\lambda(\alpha,\, t) = \frac{d\mu\left(t^{*}_{\alpha^{-1}}\right)}{d\mu(t)} = \frac{d\mu\,(t_{\alpha^{-1}})}{d\mu(t)} = \frac{\alpha^{-1} p'_{t_0}(t)}{p'_{t_0}(t_{\alpha^{-1}})}. \tag{12}$$

If the local wavelet function $\psi^{(\tau_0)}$ is bounded and compactly supported in the interval $[t_0 - \varepsilon,\, t_0 + \varepsilon] \subset I$, a shorter designation $\psi_a^{(\tau_0)}$ can be adopted to indicate the expression $D_\tau(\alpha)\psi^{(\tau_0)}(t)$, that is

$$\psi_\alpha^{(\tau_0)} := \lambda^{\frac{1}{2}}(\alpha,\, t)\psi^{(\tau_0)}(t_{\alpha^{-1}}),$$

Maximum $\alpha_{\max}$ of local dilation is $\alpha_{\max} = \alpha_{\psi^{(\tau_0)}}$, which is applicable to local wavelet $\psi_\alpha^{(\tau_0)}$.

Definition 5 Assume that a signal $s \in \mathfrak{I}(B_{(\tau)})$, its local wavelet transform at a given point τ_0 can be defined as

$$W_{\psi_\alpha^{(\tau_0)}} s = \left\langle s,\ \psi_\alpha^{(\tau_0)} \right\rangle_{\Im(B_{\tau_0})} = \int_{B_{\tau_0}} s(t)\overline{\psi_\alpha^{(\tau_0)}} dt$$
$$= \int_{B_{\tau_0}} \lambda^{\frac{1}{2}}(\alpha,\ t)\overline{\psi^{(\tau_0)}(t_{\alpha^{-1}})} s(t) dt \tag{13}$$

Further, the translation of the local wavelet $\psi^{(\tau_0)}$ at point τ_0 is defined by

$$T_\iota \psi^{(\tau_0)}(t) = \psi^{(\tau_0)} \circ p^{-1}(p(t) - p(\iota)),$$

where $\vec{\rho}(\iota) \in C$.

That translation and dilation operator can be acted on this local wavelet $\psi^{(\tau_0)}(t)$ and it yields the following expression:

$$\psi_{\alpha,\ \iota}^{(\tau_0)}(t) = \lambda^{1/2}(\alpha,\ t)\psi^{(\tau_0)} \circ p^{-1}\left(\alpha^{-1} p(t) - p(\iota)\right) \tag{14}$$

According to the Definition 5 and Eq. (14), the local wavelet transform of the signal s by dilated and translated wavelet $\psi_{\alpha,\ \iota}^{(\tau_0)}(t)$ can also be represented by the following equation:

$$W_{\psi_{\alpha,\ t}^{(\tau_0)}} s = \left\langle s,\ \psi_{\alpha,\ t}^{(\tau_0)} \right\rangle_{\Im(B_{\tau_0})} = \int_{B_{\tau_0}} s(t)\overline{\psi_{\alpha,\ t}^{(\tau_0)}} dt$$
$$= \int_{B_{\tau_0}} \lambda^{\frac{1}{2}}(\alpha,\ t)\overline{\psi^{(\tau_0)} \circ p^{-1}(\alpha^{-1} p(t) - p(t))} s(t) dt \tag{15}$$

Definition 6 Consider a square integrable function $\psi^{(\tau_0)} \in \Im(B_{(\tau_0)})$ at point τ_0, if is satisfies the following condition:

$$0 < C_{\psi^{(\tau_0)}} = \int_0^{\alpha_{\psi^{(\tau_0)}}} \frac{\|\widehat{\psi}(\omega_\alpha)\|^2}{\alpha^2} d\alpha < \infty \tag{16}$$

Then $\psi^{(\tau_0)}$ is a local mother wavelet basis on a helix, and the condition (16) is called the admissibility condition.

Theorem 1 (Local Wavelet Reconstruction) Consider a local mother wavelet function $\psi^{(\tau_0)} \in \Im(B_{(\tau_0)})$ at point τ_0, and a signal function $s \in \Im(B_{(\tau_0)})$. If $W_{\psi_{\alpha,\ \iota}^{(\tau_0)}} s(\alpha,\ \iota)$ is the LWT of the signal s at point τ_0, then for an arbitrary signal $s \in \Im(B_{(\tau_0)})$, the following equation holds:

$$C_{\psi^{(\tau_0)}} S(t) = \int_{B_{\tau_0}} \int_0^{\alpha_{\psi^{(\tau_0)}}} W_{\psi_{\alpha,\ \iota}^{(\tau_0)}} S(\alpha,\ \iota)\psi_{\alpha,\ \iota}^{(\tau_0)}(t) \frac{d\alpha}{\alpha^2} d\iota \tag{17}$$

Proof. This local wavelet reconstructing formula can be proved from the right expression.

$$\int_{B_{\tau_0}}\int_0^{\alpha_{\psi^{(\tau_0)}}} W_{\psi_{\alpha,\iota}^{(\tau_0)}} s\cdot\psi_{\alpha,\iota}^{(\tau_0)}\frac{d\alpha}{\alpha^2}d\iota$$

$$=\int_{B_{\tau_0}}\int_0^{\alpha_{\psi^{(\tau_0)}}}\left\langle s,\ \psi_{\alpha,\iota}^{(\tau_0)}\right\rangle_{\Im}\psi_{\alpha,\iota}^{(\tau_0)}\frac{d\alpha}{\alpha^2}d\iota$$

$$=\frac{1}{2\pi}\int_{B_{\tau_0}}\int_0^{\alpha_{\psi^{(\tau_0)}}}\left\langle \hat{s},\ \hat{\psi}_{\alpha}^{(\tau_0)}\right\rangle_{\Im}\psi_{\alpha,\iota}^{(\tau_0)}\frac{d\alpha}{\alpha^2}d\iota$$

$$=\frac{1}{2\pi}\int_{B_{\tau_0}}\int_0^{\alpha_{\psi^{(\tau_0)}}}\int_{B_{\tau_0}}\hat{s}(\omega)\overline{\hat{\psi}_{\alpha,\iota}^{(\tau_0)}(\omega)}d\omega\psi_{\alpha,\iota}^{(\tau_0)}\frac{d\alpha}{\alpha^2}d\iota$$

$$=\frac{1}{2\pi}\int_{B_{\tau_0}}\int_0^{\alpha_{\psi^{(\tau_0)}}}\int_{B_{\tau_0}}\hat{S}(\omega)\int_{B_{\tau_0}}e^{i\alpha p_{t_0}(\omega)\cdot\alpha^{-1}p_{t_0}(t)}\lambda(\alpha,t)\overline{\psi^{(\tau_0)}\circ p_{t_0}^{-1}\left(\alpha^{-1}\cdot p_{t_0}(t)-p_{t_0}(\iota)\right)}dtd\omega$$

$$\times\psi^{(\tau_0)}\circ p_{t_0}^{-1}\left(\alpha^{-1}\cdot p_{t_0}(t)-p(\iota)\right)\frac{d\alpha}{\alpha^2}d\iota$$

$$=\frac{1}{2\pi}\int_{B_{\tau_0}}\int_0^{\alpha_{\psi^{(\tau_0)}}}\int_{B_{\tau_0}}\hat{S}(\omega)\int_{B_{\tau_0}}e^{ip_{t_0}(\omega_\alpha)\cdot p_{t_0}\left(t_{\alpha^{-1}}^*\right)}\overline{\psi^{(\xi_0)}\left(t_{\alpha^{-1}}^*\right)}dt_{\alpha^{-1}}^*d\omega e^{i\alpha p(t)p_{t_0}(\omega)}$$

$$\times\psi^{(\xi_0)}\circ p_{t_0}^{-1}\left(\alpha^{-1}\cdot p_{t_0}(t)-p(\iota)\right)\frac{d\alpha}{\alpha^2}d\iota$$

$$=\frac{1}{2\pi}\int_{B_{\tau_0}}\int_0^{\alpha_{\psi^{(\tau_0)}}}\int_{B_{\tau_0}}\hat{s}(\omega)\overline{\hat{\psi}^{(\tau_0)}(\omega_\alpha)}d\omega e^{i\alpha p_{t_0}(\iota)p_{t_0}(\omega)}\psi^{(\tau_0)}\circ p_{t_0}^{-1}\left(\alpha^{-1}\cdot p_{t_0}(t)-p_{t_0}(t)\right)\frac{d\alpha}{\alpha^2}dt$$

$$\xlongequal{p_{t_0}\left(t^{\#}\right)=\alpha^{-1}\cdot p_{t_0}(t)-p_{t_0}(t)}\frac{1}{2\pi}\int_{B_{\tau_0}}\int_0^{\alpha_{\psi^{(\tau_0)}}}\int_C\hat{s}(\omega)\overline{\hat{\psi}(\omega_\alpha)}d\omega e^{i\alpha p_{t_0}(\omega)\left[\alpha^{-1}\cdot p_{t_0}(t)-p_{t_0}\left(t^{\#}\right)\right]}\psi^{(\tau_0)}\left(t^{\#}\right)\frac{d\alpha}{\alpha^2}dt^{\#}$$

$$=\frac{1}{2\pi}\int_{B_{\tau_0}}\hat{S}(\omega)e^{ip_{t_0}(\omega)\cdot p_{t_0}(t)}d\omega\int_0^{\alpha_{\psi^{(\tau_0)}}}\overline{\hat{\psi}^{(\tau_0)}(\omega_\alpha)}\hat{\psi}^{(\tau_0)}(\omega_\alpha)\frac{d\alpha}{\alpha^2}=C_{\psi^{(\tau_0)}}S(t)$$

where there exists a $t_{\alpha^{-1}}^*$ such that $p_{t_0}\left(t_{\alpha^{-1}}^*\right)=\alpha^{-1}\cdot p_{t_0}(t)-p(\iota)$.

4. Numerical examples

In this section, three examples are provided for discussing the LWT on a helix and its reconstruction.

Example 2 Consider a helix curve in this unit sphere, which is also defined in Example 1. The parameter formula is defined in the following expression:

$$\vec{\rho} = \{\cos t \cos 2t,\ \cos t \sin 2t,\ \sin t\},\ t \in [-1,\ 1].$$

By taking Morlet as an example, the local Morlet can be lifted onto the helix at $t = 0$ by the bijective projection of a helix curve $\vec{\rho}(t)$ in Example 1, and the function expression of Morlet wavelet is shown as

$$\psi(t) = Ce^{-\frac{t^2}{2}} \cos 5t$$

where C is a normalized constant. Some figures are given for our discussion in Figure 4. The Figure 4a shows the figure of the Morlet wavelet, and the Figure 4b gives the figure of the local Morlet mapped onto the helix at $t = 0$ within unit spherical perspective. For comparison, the figure of the projected local Morlet wavelet is shown in Figure 4c without unit spherical perspective.

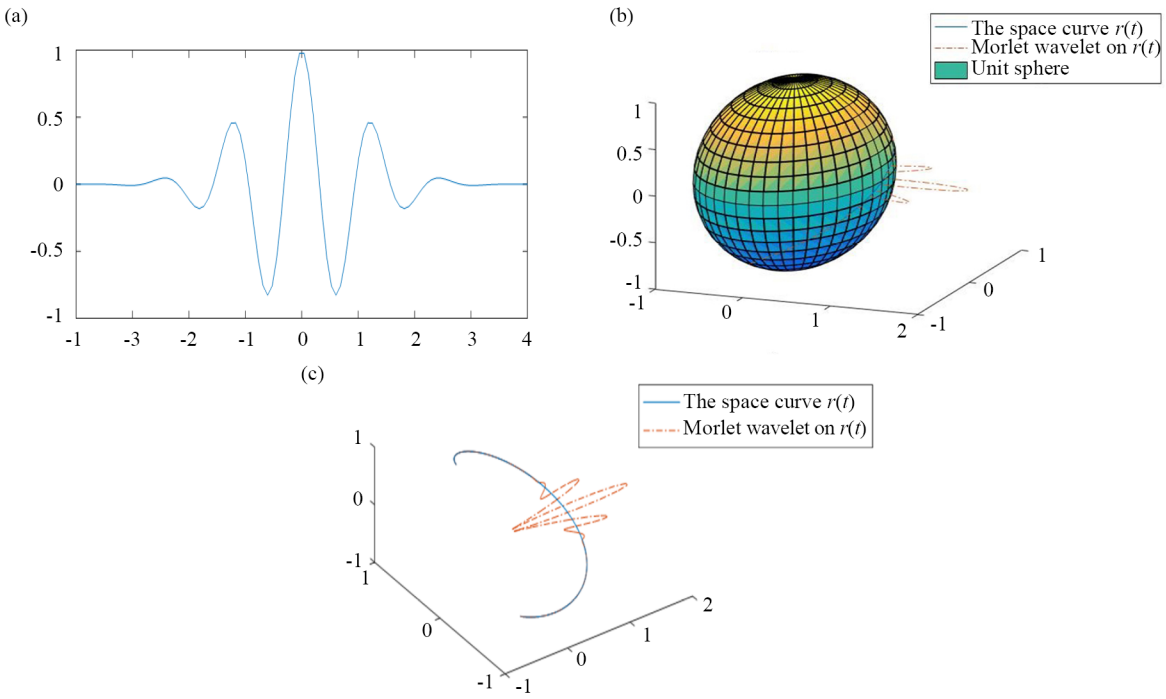

Figure 4. Morlet wavelet and local Morlet wavelet at point $t = 0$. (a) Morlet wavelet; (b) Morlet wavelet lifted onto the helix curve within spherical perspective; (c) Morlet wavelet lifted onto the helix curve without spherical perspective

Consider a signal $s(t)$ on this helix at $t = 0$. The projected signal on its tangent line is given as the following expression:

$$s(T) = 0.2\cos(10T) + 0.1\sin(50T),\ T \in [-0.49,\ 0.49]. \tag{18}$$

This local signal $s(T)$ can also be projected onto the helix by this inverse of projection P defined as the Eq. (6). The helix curve $\vec{\rho}(t)$ is given by a blue curve in Figure 5a and 5b. Figure 5a shows figures within unit spherical perspective

and Figure 5b shows the corresponding figures without unit spherical perspective. The raw signal on helix curve oscillates in the neighborhood at point $t = 0$. Based on the Matlab routine [12, 15] with respect to Continuous Wavelet Transform (CWT) and local reconstruction formula in the Theorem 1, reconstructed signal on helix curve $\vec{\rho}(t)$ can be calculated and shown in Figure 5c and 5d. Figure 5c shows figures within unit spherical perspective and Figure 5d shows the corresponding figures without unit spherical perspective.

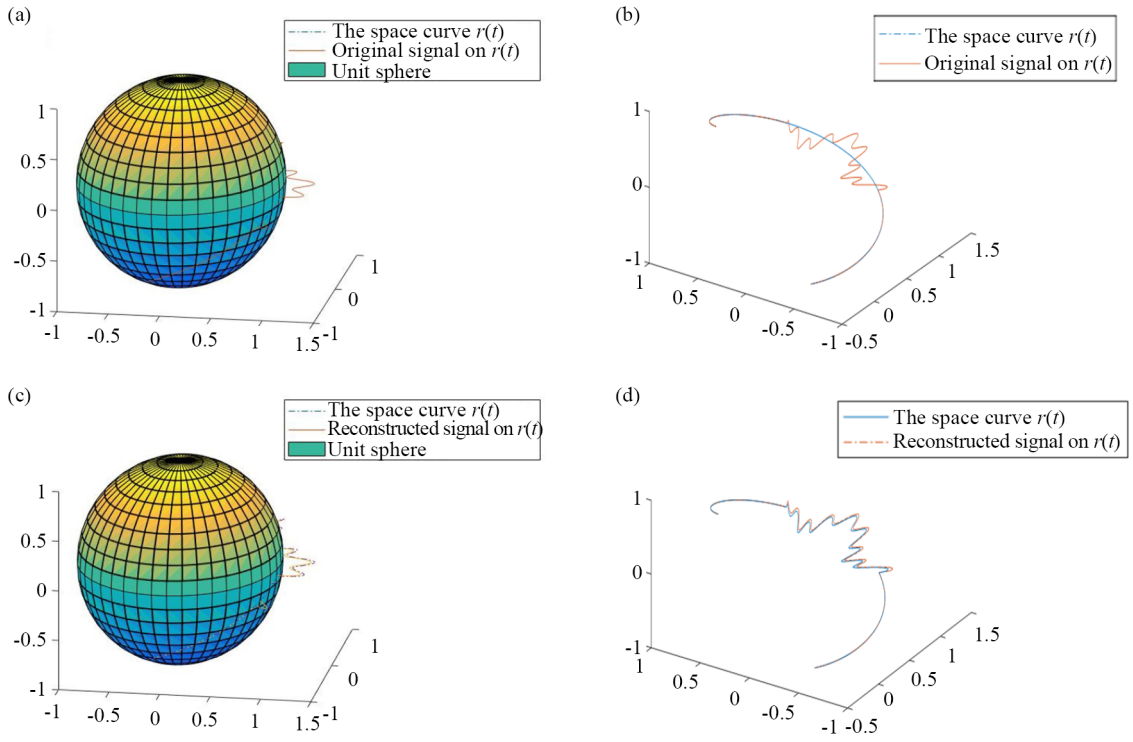

Figure 5. Local signal $s(T)$ and the reconstructed signal on this helix. (a) original signal within unit spherical perspective; (b) original signal without unit spherical perspective; (c) reconstructed signal within unit spherical perspective; (d) reconstructed signal without unit spherical perspective

Example 3 Consider a helix curve defined in Example 1. Its parameter formula is also given in the following expression:

$$\vec{\rho} = \{\cos t \cos 2t,\ \cos t \sin 2t,\ \sin t\},\ t \in [-1,\ 1].$$

By taking the Mexihat as an example similarly, an local Mexihat can also be mapped onto the helix at $t = 0$ by its bijective projection of a helix curve $\vec{\rho}(t)$ in Example 1. Some figures are shown to discuss the results of simulation in Figure 6. The Figure 6a reveals the figure of the Mexihat, and the Figure 6b exhibits the figure of the local Mexihat mapped onto this helix at $t = 0$ within unit spherical perspective. For comparison, the figure of the projected local Mexihat wavelet is shown in Figure 6c without unit spherical perspective. The results are shown in the Figure 6. A graph of the Mexihat are shown in the top graph of Figure 6, and the bottom graph of Figure 6 shows the figure of the local Mexihat mapped onto this helix at $t = 0$.

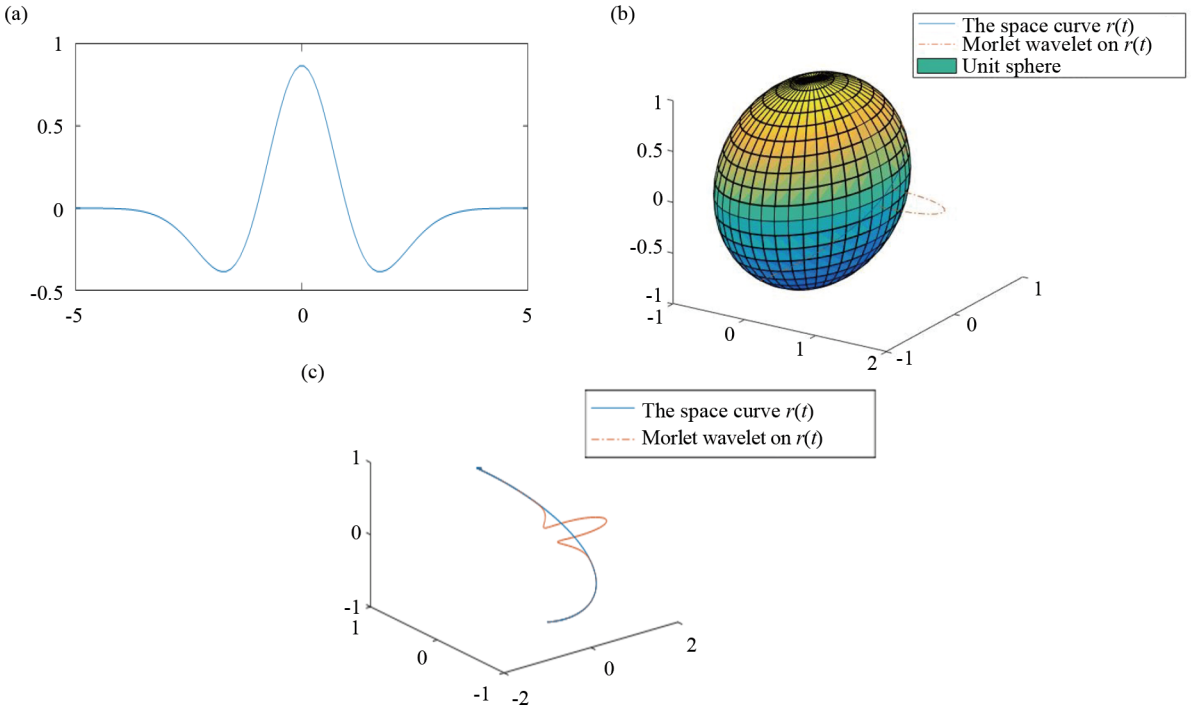

Figure 6. Mexihat and local Mexihat at $t = 0$. (a) Morlet wavelet; (b) Mexihat wavelet lifted onto the helix curve within spherical perspective; (c) Mexihat wavelet lifted onto the helix curve without spherical perspective

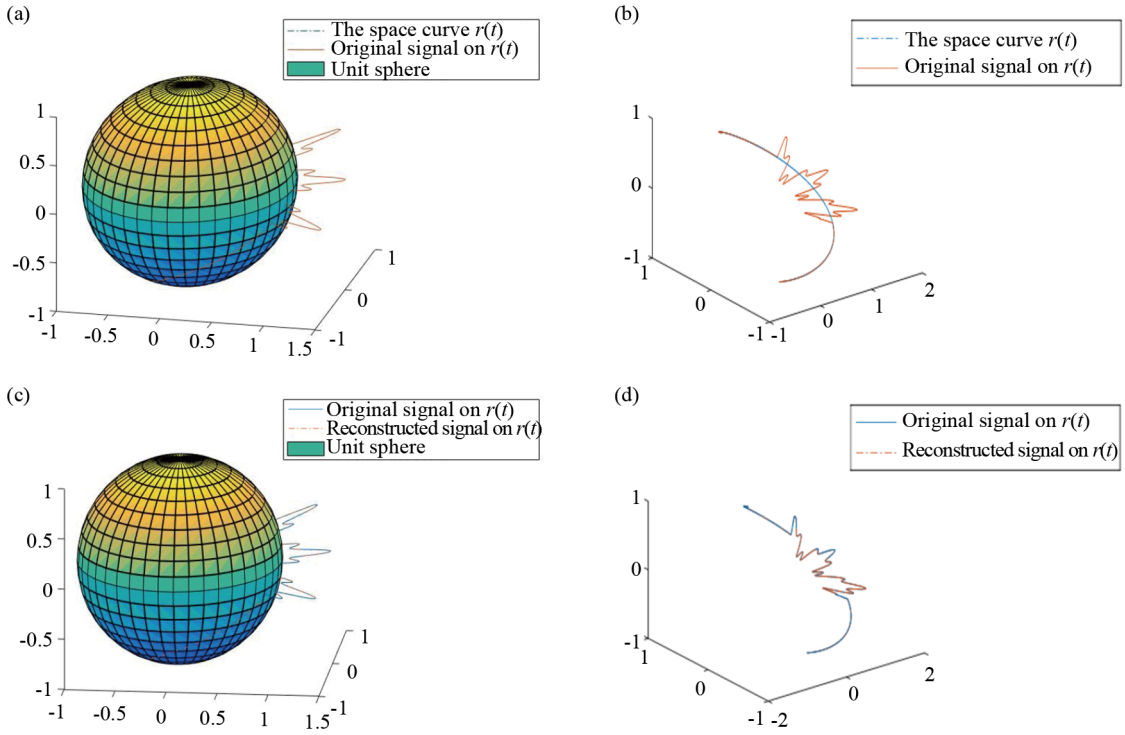

Figure 7. Original signal and its reconstruction signal on the helix curve. (a) original signal within unit spherical perspective; (b) original signal without unit spherical perspective; (c) reconstructed signal within unit spherical perspective; (d) reconstructed signal within unit spherical perspective

Consider a signal $s(t)$ on this helix at $t = 0$. The projected signal on its tangent line is given as the following expression:

$$s(T) = 0.32\sin(8T) + 0.15\cos(32T) \tag{19}$$

where $T \in [-1,\ 1]$. The local signal $s(T)$ can be projected onto the helix curve by the inverse of projection P defined as the Eq. (6). The helix curve $\vec{\rho}(t)$ is shown by the blue curve in Figure 7a and 7b. Figure 7a shows figures within unit spherical perspective and Figure 7b shows the corresponding figures without unit spherical perspective. The raw signal on helix curve oscillates in the neighborhood at point $t = 0$. Based on the Matlab routine [12, 15] with respect to CWT and local reconstruction formula in the Theorem 1, reconstructed signal on helix curve $\vec{\rho}(t)$ can be calculated and shown in Figure 7c and 7d. Figure 7c shows figures within unit spherical perspective and Figure 7d shows the corresponding figures without unit spherical perspective.

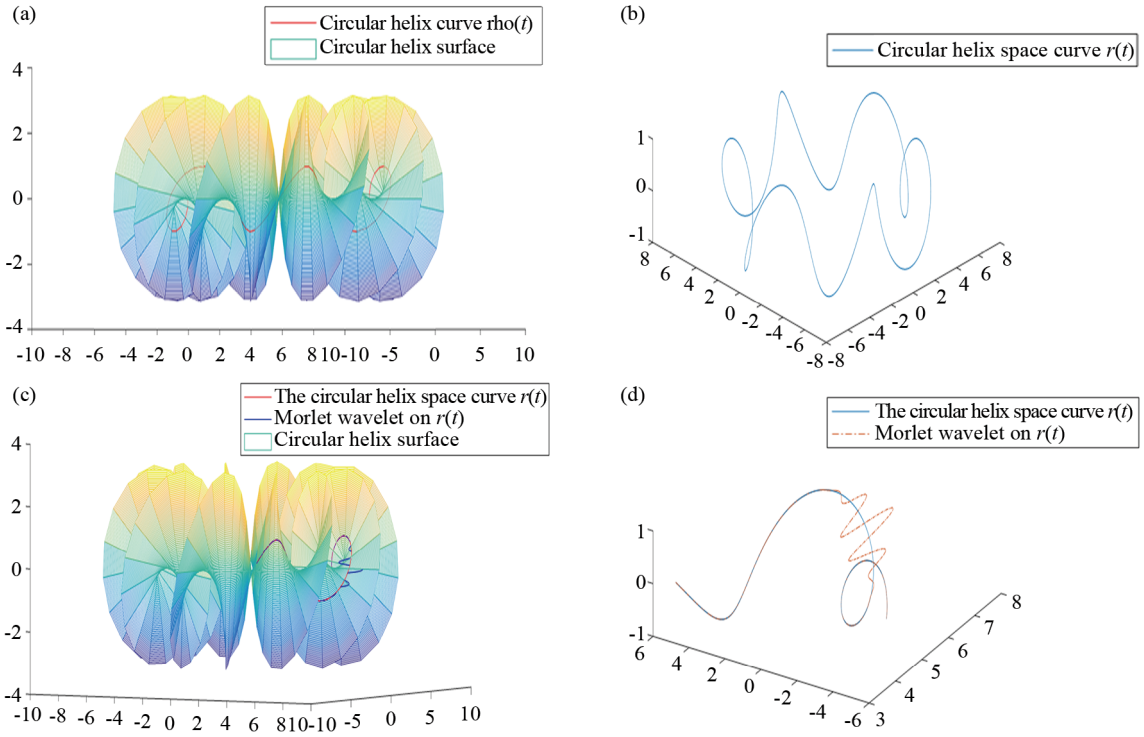

Figure 8. Morlet wavelet, circular helix curve and local Morlet at $t = 0$. (a) circular helix curve within circular helix surface perspective; (b) circular helix curve without circular helix surface perspective; (c) local Morlet wavelet within circular helix surface perspective; (d) local Morlet wavelet without circular helix surface perspective

Example 4 According to the parameter equation defined in Definition 1, consider a circular helix curve, and its parameter formula is also given in the following expression:

$$\vec{\rho} = \{(6+\cos 6t)\cos t,\ (6+\cos 6t)\sin t,\ \sin 6t\}, \tag{20}$$

where $t \in [-\pi,\ \pi]$. This circular helix is on a corresponding circular helix surface. Choose a point $t_0 = 0$ and its neighbourhood $(-1,\ 1)$. The tangent projection at point $t_0 = 0$ can be computed, similarly to the discussion in section

2.2. By choosing the Morlet wavelet which can be seen in Example 2, an local Morlet at $t = 0$ can be projected onto the circular helix $\vec{\rho}(t)$. For a visual observation, the figures are shown in the Figure 8. The Figure 8a shows the figure of the circular helix curve in Eq. (20) within circular helix surface perspective, and the Figure 8b gives the circular helix curve in Eq. (20) without circular helix surface perspective. The Figure 8c shows the local Morlet's figure which is projected onto this helix curve at $t = 0$ within circular helix surface perspective. The Figure 8d shows the Morlet's graph without circular helix surface perspective.

Consider a signal $s(t)$ on this helix curve at point $t = 0$. The projected signal $s(T)$ on its tangent line is given as the following expression:

$$s(T) = 0.2\cos(10T) + 0.1\sin(50T),\ T \in [-1,\ 1] \tag{21}$$

The raw signal $s(T)$ can also be mapped onto the circular helix $\vec{\rho}(t)$. The local helix curve $\vec{\rho}(t)$ in the interval $[-1,\ 1]$ is shown by the red curve in the Figure 9a within circular helix surface perspective. The raw signal mapped on the circular helix $\vec{\rho}(t)$ at $t = 0$ is given by the blue curve in the Figure 9b. Figure 9b shows local helix curve $\vec{\rho}(t)$ in the interval $[-1,\ 1]$ and the original signal $s(t)$ without circular helix surface perspective, respectively. The raw signal on this helix oscillates in a neighborhood at point $\vec{\rho}(t)$. Based on the Matlab routine [12, 15] with respect to CWT and local reconstruction formula in the Theorem 1, reconstructed signal on helix curve $\vec{\rho}(t)$ can be calculated and shown in Figure 9c and 9d. Figure 9c shows the results within circular helix surface perspective and Figure 9d shows the corresponding figures without circular helix surface perspective.

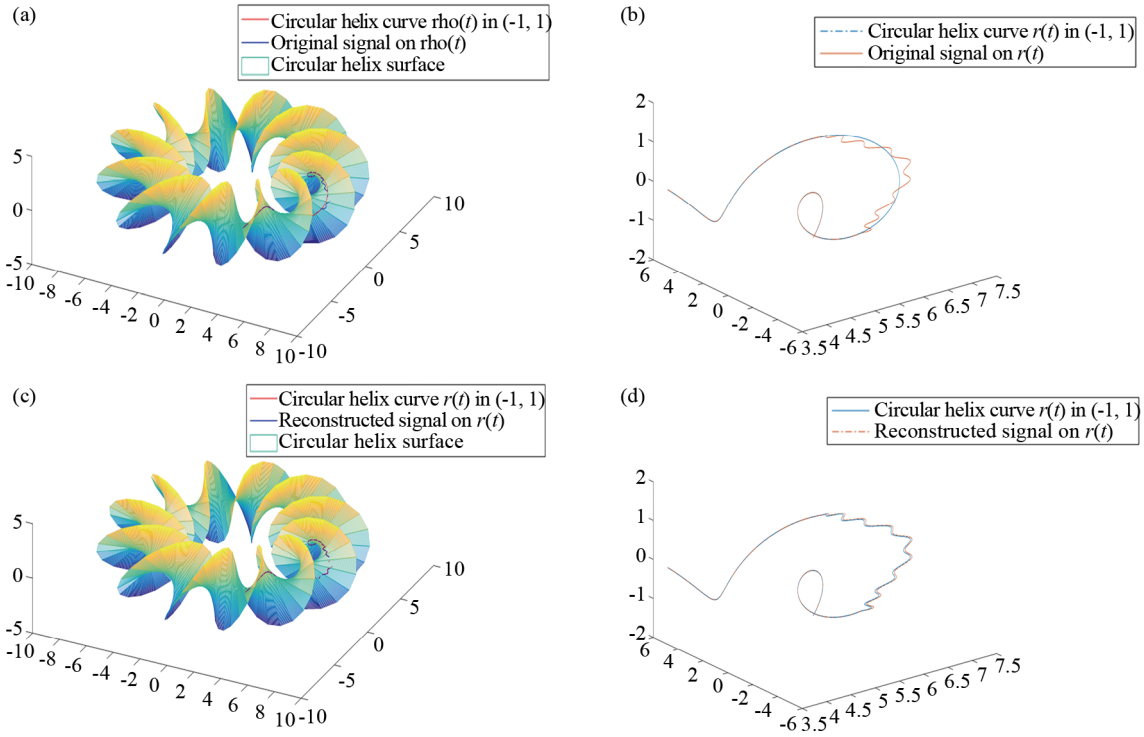

Figure 9. Raw signal and the corresponding reconstruction signal on a circular helix. (a) raw signal within circular helix surface perspective; (b) raw signal without circular helix surface perspective; (c) reconstructed signal within circular helix surface perspective; (d) reconstructed signal without circular helix surface perspective

Moreover, the errors between three dimensional raw signal and the reconstructed signal is calculated in the above three examples. The Mean Square Error (MSE) are listed in Table 1. The vector α, β and γ of Frenet frame are established as X-axis, Y-axis and Z-axis at point $t = 0$ of helix curves respectively. So the total MSE, MSE in part of X-axis, MSE in part of Y-axis and MSE in part of Z-axis are computed for Example 2-4 respectively. These results implicate the error of local wavelet transform. And MSE in part of X-axis are bigger compared to MSE in part of Y-axis and MSE in part of Z-axis. These mean that the error between the raw signal on a helix and its reconstructed signal by LWT is small but it needs to be further reduced to meet the requirements of practical applications. The error in part of X-axis dominates the main part of the error, compared the part of Y-axis and part of Z-axis. In order to reduce the error, perhaps we might consider updating the local projection, improving the accuracy of local adjacent structures for a helix at some point and other methods in future studies.

Table 1. MSE between original signal and reconstructed signal

	Example 2	Example 3	Example 4
Total MSE	3.5697×10^{-04}	5.9401×10^{-06}	3.9779×10^{-05}
MSE in part of X-axis	3.1447×10^{-04}	5.3443×10^{-06}	3.8384×10^{-05}
MSE in part of Y-axis	3.3425×10^{-05}	4.6874×10^{-07}	8.9534×10^{-07}
MSE in part of Z-axis	9.0726×10^{-06}	1.2707×10^{-07}	4.9948×10^{-07}

5. Conclusion

In this paper, a rigorous mathematical framework is developed for analyzing helix curves through local wavelet transform methodologies, with particular emphasis on helical geometries. Three-dimensional parametric helix curves are formally characterized including circular helix and generalized helix. Every point of helix curves admits orthogonal projection onto its tangent line at a given point t_0. To enable data analysis on such manifolds, we propose a local projection operator that facilitates the definition of Local Wavelet Transform (LWT) on the helix curve, formally expressed as a dilated and translated wavelet. The reconstruction formula is rigorously established signal recovery under admissibility conditions. Three numerical examples confirms the method's efficacy in processing non-uniformly sampled signals along helical trajectories by employing Morlet and Mexican hat wavelets, with mean squared error below in reconstruction accuracy. The discussed methodology preserves the intrinsic geometric structure through projection-lifting operations, enabling faithful extension to arbitrary helix curves. Future work will investigate adaptive wavelet dictionaries incorporating Frenet-Serret frame coefficients to enhance directional sensitivity, with potential applications in geometric deep learning and medical image analysis on tubular structures.

Conflict of interest

The authors declare no competing financial interest.

References

[1] You X, Li Q, Tao D, Ou W, Gong M. Local metric learning for exemplar-based object detection. *IEEE Transactions on Circuits and Systems for Video Technology*. 2014; 24(8): 1265-1276.

[2] Zhang D, You X, Wang P, Yanushkevich SN, Tang YY. Facial biometrics using non-tensor product wavelet and 2D discriminant techniques. *International Journal of Pattern Recognition and Artificial Intelligence*. 2009; 23(3): 1-21.

[3] Antoine JP, Daniela R, Vandergheynst P. Wavelet transform on manifolds: Old and new approaches. *Applied and Computational Harmonic Analysis*. 2010; 28(2): 189-202.

[4] Zhou X, Wang B. Wavelet analysis on some smooth surface with nonzero constant Gaussian curvature. *International Journal of Wavelets, Multiresolution and Information Processing*. 2018; 16(1): 1850007.
[5] Zhou X. Wavelet transform on regression trend curve and its application in financial data. *International Journal of Wavelets, Multiresolution and Information Processing*. 2020; 18(5): 2050040.
[6] Zhou X, Wang G. Biorthogonal wavelet on a logarithm curve ℂ. *Journal of Mathematics*. 2021; 2021: 7985069.
[7] Singh AK, Bhate H. Stochastic wavelets from minimizers of an uncertainty principle: An example. *International Journal of Wavelets, Multiresolution and Information Processing*. 2020; 18(6): 2050046.
[8] Leduc JP. Spatio-temporal wavelet transforms for digital signal analysis. *Signal Processing*. 1997; 60(1): 23-41.
[9] Kikuchi K, Wang B. Spatiotemporal wavelet transform and the multiscale behavior of the Madden-Julian oscillation. *Journal of Climate*. 2010; 23(14): 3814-3834.
[10] Mujica F, Leduc JP, Smith MJT, Murenzi R. Spatiotemporal wavelets: A group-theoretic construction for motion estimation and tracking. *SIAM Journal on Applied Mathematics*. 2000; 61(2): 596-632.
[11] Zhou X. Yi lei guang yi luo mian de fang cheng yu tu shi [The equation and figures of a class of generalized helicoid]. *Journal of Suzhou University*. 2016; 31(3): 93-95.
[12] Zhou X. Wavelet analysis on a generalized helix space curves and its examples. *EURASIP Journal on Advances in Signal Processing*. 2024; 2024(1): 70.
[13] Miyashita S, Nogami K. *Wei Fen Ji He Ji Chu [Fundamentals of Differential Geometry]*. Vol. 1. China: Science Press; 2010.
[14] Mei X, Huang J. *Wei Fen Ji He [Differential Geometry]*. 4th ed. China: Higher Education Press; 2008.
[15] Erickson J. *Continuous Wavelet Transform and Inverse*. MATLAB Central File Exchange; 2022. Available from: https://www.mathworks.com/matlabcentral/fileexchange/20821-continuous-wavelet-transform-and-inverse [Accessed 20th May 2025].